Mass-analyzed threshold ionization spectroscopy of lanthanide imide LnNH (Ln = La and Ce) radicals from N–H bond activation of ammonia

Yuchen Zhang, Silver Nyambo, and Dong-Sheng Yang

Citation: J. Chem. Phys. **149**, 234301 (2018); doi: 10.1063/1.5064597
View online: https://doi.org/10.1063/1.5064597
View Table of Contents: http://aip.scitation.org/toc/jcp/149/23
Published by the American Institute of Physics

Mass-analyzed threshold ionization spectroscopy of lanthanide imide LnNH (Ln = La and Ce) radicals from N–H bond activation of ammonia

Yuchen Zhang, Silver Nyambo, and Dong-Sheng Yang[a)]
Department of Chemistry, University of Kentucky, Lexington, Kentucky 40506-0055, USA

(Received 5 October 2018; accepted 23 November 2018; published online 17 December 2018)

Ln (Ln = La and Ce) atom reactions with ammonia are carried out in a pulsed laser vaporization supersonic molecular beam source. Lanthanide-containing species are observed with time-of-flight mass spectrometry, and LnNH molecules are characterized by mass-analyzed threshold ionization (MATI) spectroscopy and quantum chemical calculations. The theoretical calculations include density functional theory for both Ln species and a scalar relativity correction, electron correlation, and spin-orbit coupling for the Ce species. The MATI spectrum of LaNH exhibits a single vibronic band system with a strong origin band and two weak vibronic progressions, whereas the spectrum of CeNH displays two band systems separated by 75 cm^{-1} with each being like the LaNH spectrum. By comparing with the theoretical calculations, both LaNH and CeNH are identified as linear molecules with $C_{\infty v}$ symmetry, and the two vibronic progressions are attributed to the excitations of Ln–N stretching and Ln–N–H bending modes in the ions. The additional band system observed for CeNH is due to the spin-orbit splitting from the interactions of triplet and singlet states. The ground valence electron configurations of LaNH and CeNH are La $6s^1$ and Ce $4f^16s^1$, and the ionization of each species removes the Ln $6s^1$ electron. The remaining two electrons that are associated with the isolated Ln atoms or ions are in a doubly degenerate molecular orbital that is a bonding combination between Ln $5d_\pi$ and N p_π orbitals. *Published by AIP Publishing.* https://doi.org/10.1063/1.5064597

I. INTRODUCTION

Bond activation of ammonia by metal atoms or ions has attracted considerable interest in gas-phase and solid-argon chemistry and spectroscopy. Such interest could be associated with the development of fundamental chemistry in oxidative addition of ammonia,[1,2] catalytic C–H amination,[2–4] or ammonia as a feedstock for producing hydrogen in fuel cells.[5] Metal ion reactions in the gas phase have largely been investigated with mass spectrometry-based techniques.[6–17] It has been reported that reactions of the early transition metal ions (M^+ = Sc^+, Ti^+, and V^+) are exothermic and produce $[MNH]^+$, while reactions of the middle and late transition metal ions (M^+ = Cr^+–Cu^+) at their ground electronic states are endothermic and could yield $[MNH_{1,2}]^+$ or $[MH]^+$ ions.[17] For lanthanide ions (Ln^+), H_2 elimination to form $[LnNH]^+$ is observed with La^+, Ce^+, Gd^+, and Tb^+ and NH_3 addition with all other Ln^+ ions (except for Pm^+).[11,12] For neutral metal atom reactions in the gas phase, MNH_3 (M = Al, Ga, and In)[18–20] and $M(NH_3)_{1,2}$ (M = Cu and Ag)[21–24] have been characterized with zero electron kinetic energy or resonantly enhanced two photon ionization spectroscopy and MNH (M = Sc, Y, and La) with a fast-flow reactor,[25] laser-induced fluorescence,[26–29] or optical Stark spectroscopy.[30] In solid Ar matrices, neutral metal atom reactions have been investigated with matrix isolation infrared spectroscopy.[31–39] It has been shown that laser-ablated metal atoms (M = Sc, Ti, V, Zr, Hf, Cr, Mo, Ta, Ce, Th, and U) react with ammonia to form MNH_3 spontaneously on annealing. The MNH_3 complexes undergo photochemical rearrangement to $HMNH_2$, and the $HScNH_2$ molecule further decomposes to ScNH + H_2 upon ultraviolet-visible irradiation.[33] On the other hand, for the Ce atom reaction, the H_2CeNH molecule decomposes to yield HCeN + H_2 upon photolysis.[38,39] The observation of HCeN in Ar matrices is interesting though a bit surprising because the decomposition of H_2MNH requires additional energy to break the remaining N–H bond, and other rare earth reactions with NH_3 have been reported to produce MNH (M = Sc, Y, and La) in the gas phase[26–30] and in Ar matrices (M = Sc).[33]

In this article, we report the observation of Ln atoms (Ln = La and Ce)-mediated H_2 elimination of NH_3 and spectroscopic and computational characterization of the LnNH radicals formed in the Ln + NH_3 reactions. The motivation of this work was to compare the reactions of two Ln metals under similar experimental conditions and the spectroscopy and structures of the resultant Ln radicals. La atoms have the ground electron configuration $[Xe]5d6s^2$ and a low-energy reactive configuration $[Xe]5d^26s^1$ at 7.6 kcal/mol. Similarly, Ce atoms have the ground electron configuration $[Xe]4f^15d^16s^2$ and a low-energy reactive configuration $[Xe]4f^15d^26s^1$ at 6.8 kcal/mol. Because 4f orbitals of the Ln atoms penetrate the xenon core and are traditionally thought to be unable to overlap with ligand orbitals,[40] both La and Ce reactions with ammonia are expected to produce similar products. However, the recent matrix-isolation infrared

a)Author to whom correspondence should be addressed: dyang0@uky.edu

spectroscopic studies proposed that the dehydrogenation species formed by the Ce + NH_3 reaction in solid Ar[38,39] had a different structure (HCeN) from that produced by the La + NH_3 reaction in the gas phase (LaNH).[29,30] The variation could be due to different experimental conditions used in the previous studies or the inherent difference of the two elements. Thus, it is desirable to investigate the two reactions and their products in the same medium and under similar experimental conditions. Moreover, the presence of a 4f electron is expected to yield additional electronic energy levels and thus more complex spectroscopy due to the closely lying 4f orbitals and spin-orbit (SO) coupling. This study was set out to address the above two propositions.

II. EXPERIMENTAL AND COMPUTATIONAL METHODS

A. Experimental

The metal-cluster beam instrument used in this work consists of reaction and spectroscopy vacuum chambers and was described in a previous publication.[41] The Ln-ammonia reactions were carried out in a laser vaporization metal cluster beam source. NH_3 (99.98%, Aldrich) was seeded in He carrier gas (99.998%, Scott Gross) with a concentration of 0.4% in a stainless-steel mixing cylinder. La and Ce atoms were generated by pulsed-laser (Nd:YAG, Continuum Minilite II, 532 nm, ~2 mJ/pulse) vaporization of a La or Ce rod (99%, Metallium) in the presence of the NH_3/He mixture (40 psi) delivered by a home-made piezoelectric pulsed valve. The metal atoms and the gas mixture entered a collision tube (2 mm diameter and 2 cm length) and were then expanded into the reaction chamber, collimated by a cone-shaped skimmer (2 mm inner diameter) and passed through a pair of deflection plates. Ionic species in the molecular beam that were formed during laser vaporization were removed by an electric field (100 V cm^{-1}) applied on the deflection plates. The neutral products were identified by photoionization time-of-flight mass spectrometry.

Prior to the mass-analyzed threshold ionization (MATI) measurements, photoionization efficiency spectra of LnNH were recorded to locate their approximate ionization thresholds to guide MATI scans. In the MATI experiment, the Ln molecules were excited to high-lying Rydberg states in a single-photon process and ionized by a delayed pulsed electric field. The excitation laser was the same as that for photoionization in the mass spectrometric and photoionization efficiency experiments and was the frequency doubled output of a tunable dye laser (Lumonics HD-500), pumped by the third harmonic output (355 nm) of a Nd:YAG laser (Continuum Surelite II). The laser beam was collinear and counter propagated with the molecular beam. The ionization pulsed field (320 V cm^{-1}) was generated by two high voltage pulse generators (DEI, PVX-4140) and delayed by 20 μs from the laser pulse by a delayed pulsed generator (SRS, DG641). A small DC field (4.8 V cm^{-1}) was applied to separate the ions produced by direct photoionization from the MATI ions generated by delayed field ionization. The MATI ion signal was obtained by scanning the wavelength of the tunable dye laser, detected by a dual microchannel plate detector, amplified by a preamplifier (SRS, SR445), visualized by a digital oscilloscope (Tektronix TDS 3012), and stored in a laboratory computer. Laser wavelengths were calibrated against vanadium atomic transitions in the MATI spectral region. The Stark shift on the ionization energy (IE) induced by the DC separation field was calculated using the relation $\Delta IE = 6.1E_f^{1/2}$, where E_f is in V cm^{-1} and ΔIE is in cm^{-1}.

B. Computational

The density functional theory (DFT) method with the Becke's three-parameter hybrid functional with the correlation functional of Lee, Yang, and Parr (B3LYP) was used to calculate the equilibrium geometries and vibrational frequencies of LnNH and $LnNH^+$. The basis sets used in these calculations were 6-311+G (d, p) for C and H and the Stuttgart/Dresden (SDD) effective-core-potential basis set with 28 electron cores for La and Ce. The C_s point group was used in geometry optimizations of the LnNH molecules; each was converged to a $C_{\infty v}$ linear structure. In predicting reaction pathways, the geometry of each stationary point was obtained through a relaxed potential energy surface scan along the proposed reaction coordinates. The relaxed scan involved the scanning of bond distances for bond breakage, and the structure of each point of the scan was optimized using the Berny algorithm. For each optimized stationary point, a vibrational analysis was performed to identify the nature of the stationary point. Energy minima connected by a transition state (TS) were confirmed by intrinsic reaction coordinate calculations. All DFT calculations were performed with the Gaussian 09 software package.[42]

To compare with the experimental MATI spectra, multidimensional Franck-Condon (FC) factors were calculated from the equilibrium geometries, harmonic vibrational frequencies, and normal coordinates of the neutral and ionized complexes.[43] In these calculations, recursion relations were employed, and the Duschinsky effect was considered to account for a possible axis rotation from the neutral complex to the cation. Spectral simulations were obtained using the experimental line width and the Lorentzian line shape. Transitions from excited vibrational levels of the neutral molecule were considered by assuming thermal excitation at specific temperatures.

Relativistic quantum chemical computations on CeNH and its singly charged cation were carried out to account for the observed two band systems in the MATI spectrum. These calculations involved two steps: the first step included scalar relativity corrections in the self-consistent field (SCF) process and the second step included the additional Breit-Pauli operator as a perturbation in the final SO coupling computations. Scalar relativity was incorporated into the calculations using the local unitary transformation (LUT) approximation[44] for the infinite order two component (IOTC) transformations[45,46] of the one electron integrals. The orbital bases used in these calculations were quadruple zeta-quality core-correlating (QZC) all-electron basis sets of Noro and co-workers.[47,48] Since only *spdfg* basis sets could be used in the gradient calculations, the 3*h* and 1*i* functions in the standard QZC basis for Ce were truncated from all calculations, but the full QZC bases for C and H were retained. This basis set family has correlating functions for the valence and all upper core orbitals of Ce

(as well as the 1*s* of N) so that the only orbitals excluded from correlation treatments were the deep core of Ce (1*s*, 2*sp*, 3*spd* shells). Equation of motion coupled-cluster single double (EOM-CCSD) calculations[49] based on high-spin restricted open shell SCF (ROHF)[50] wavefunctions were used to survey the excited states of both the neutral molecule and the cation. Because of computational limitations, these EOM-CCSD calculations employed the double zeta core (DZC) correlating basis set.[47,48] SO calculations were based on small configuration interaction calculations, whose orbitals were obtained using the state-averaged multi-configuration self-consistent field (MCSCF) method.[51] In these MCSCF calculations, the active spaces were two electrons in eight orbitals (2, 8) for the neutral radical with Ce $4f^16s^1$ electrons and one 6s and seven 4f orbitals, and (1, 7) for the ion with a Ce $4f^1$ electron and seven 4f orbitals. Dynamic correlation effects and spin-orbit effects were treated as simultaneous perturbations by multi-reference quasi-degenerate perturbation theory (MCQDPT).[52,53] The SO calculations used the full Breit-Pauli operator.[54,55] All relativistic calculations were performed using the General Atomic and Molecular Electronic Structure System (GAMESS) quantum chemistry package.[56]

III. RESULTS AND DISCUSSION

A. TOF mass spectra and lanthanide-containing radicals

Figure 1 displays the TOF mass spectra of the Ln + NH_3 (Ln = La and Ce) reactions recorded with 239 nm photoionization. For the La + NH_3 reaction, the mass spectrum [Fig. 1(a)] shows $LaNH(NH_3)_{0\text{-}3}$ and $LaO(NH_3)_{0\text{-}3}$. LaNH is apparently due to the H_2 elimination of NH_3, and the resultant LaNH molecule further proceeds with NH_3 associations. LaO could be formed by La reactions with oxygen that is present in the He carrier gas as an impurity or by laser vaporization of the La oxide impurity in the La rod. The fact that no La/NH_3 adducts are observed indicates that atomic La is more reactive than either LaNH or LaO toward ammonia. The products of the La + NH_3 reaction are comparable to those of the corresponding La^+ reaction observed by inductively coupled plasma mass spectrometry.[11,12] The mass spectrum of the Ce + NH_3 reaction is similar to that of the corresponding La reaction though the larger NH_3 adducts are not clearly observed. The observation of CeNH and its adducts with NH_3 in both reactions suggest that La and Ce behave similarly toward ammonia. In the discussion above, we implicitly assume that the two dehydrogenated metal-containing species have the same atomic connectivity LnNH, rather than NLnH. In the discussion below, we will show that this is indeed the case.

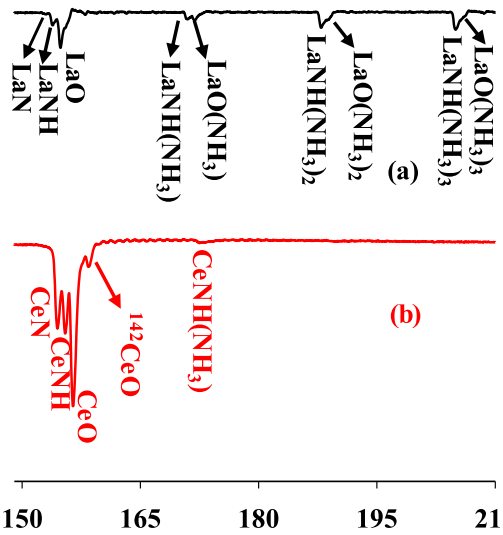

FIG. 1. TOF mass spectra of the molecular beams produced by La + NH_3 (a) and Ce + NH_3 (b) reactions recorded at 239 nm. The seeding concentration of ammonia in He was 0.4%.

B. MATI spectrum of LaNH

The MATI spectrum of LaNH [Fig. 2(a)] shows a strong origin band at 40 883 (5) cm^{-1}, which corresponds to the adiabatic IE of the molecule. Above the origin band, it displays a main progression of 808 cm^{-1} with up to two vibrational quanta, a small band at 68 cm^{-1} from each member of the main progression, a weaker progression of 526 cm^{-1} with up to two vibrational quanta as well, and a combination band of (808 + 526) cm^{-1} marked with "*". At the lower energy side of the origin band are two weak bands at 458 and 763 cm^{-1}, respectively. The 808 and 526 cm^{-1} progressions and the combination band above the origin band correspond to the transitions from the vibronic ground state of the neutral molecule to vibrational excited levels of the singly charged ion, while the satellite bands are sequence bands, and the bands below the origin band are hot bands from thermally excited vibrational levels of the neutral molecule. Thus, the 458 and 763 cm^{-1} transitions could be compared to the vibronic bands observed in the dispersed fluorescence spectrum of the $C^2\Pi \rightarrow X^2\Sigma$ transition,[29] which showed a strong ν_2 (σ^+, La–N stretch) fundamental at 750 (12) cm^{-1}, a weak ν_3(π, La–N–H bend) fundamental at 493 cm^{-1}, and a median $2\nu_2$ at 909 (9) cm^{-1} (the original paper incorrectly labeled ν_2 for the bending mode

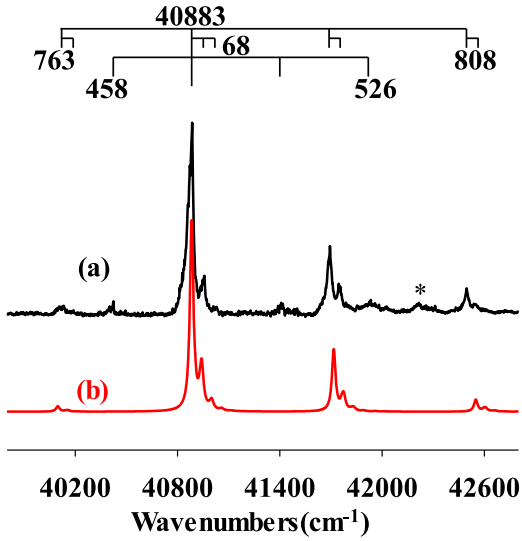

FIG. 2. MATI spectrum (a) and simulation of $^1\Sigma^+ \leftarrow {}^2\Sigma^+$ at 350 K (b) of LaNH. The energy and intensity of the origin band are aligned with or normalized to those of the experimental origin band. The band marked with "*" is a combination band of 526 + 808 cm^{-1}.

and ν_3 for the stretching mode). The weak ν_3 bending fundamental band could imply a degree of vibronic coupling in the $C^2\Pi$ state (i.e., the Renner-Teller effect). The 763 cm^{-1} hot band in our MATI spectrum is comparable to the ν_2 stretching fundamental (750 cm^{-1}) reported from the fluorescence spectrum by considering the measurement uncertainty. The 458 cm^{-1} hot band is smaller than the ν_3 fundamental from the fluorescence measurement (493 cm^{-1}) but is about one half of the ν_3 two-quantum transition (909 cm^{-1}) from the same study. Because of the weak, broad ν_3 fundamental signal in the fluorescence spectrum, it is possible that the measurement of the fundamental band position may have a larger error. Thus, we assign the two hot bands at 458 and 763 cm^{-1} in our MATI spectrum to the ν_3 and ν_2 fundamentals. Although there has been no previous vibronic measurements on $LaNH^+$, the 526 and 808 cm^{-1} vibronic bands can be assigned to ν_3^+ and ν_2^+ in the ion because the only other mode of the ion, ν_1^+ (σ^+, N–H stretch), has a much higher frequency. The difference between ν_3^+ and ν_3 (526 – 458 cm^{-1}) equals the 68 cm^{-1} separation between the 808 cm^{-1} progression and the small satellite bands. Thus, these small bands are attributed to sequence transitions between the first excited quantum of ν_3 and ν_3^+. The vibrational assignments and electronic transition are further discussed below by comparing with the theoretical calculations.

The observed MATI spectrum is attributed to the $^1\Sigma^+ \leftarrow {}^2\Sigma^+$ transition of LaNH. The ground electronic state of LaNH is predicted by the DFT calculations to be $^2\Sigma^+$ ($C_{\infty v}$), in consistent with the previous dispersed fluorescence spectroscopic study.[29] The valence electron configuration in the ground state is $\pi^4(\sigma^+)^1$, where σ^+ is a La 6s-based orbital and π^4 is a doubly degenerated bonding orbital between La $5d_\pi$ and N $2p_\pi$ (Fig. 3). Ionization removes the La 6s-based electron and yields the singlet ion state $^1\Sigma^+$. Ionization could also remove a π electron, but the resultant triplet or open-shell singlet states are expected to be considerably less stable. Because the La 6s-based electron is largely a non-bonding electron, its removal has a small effect on the molecular geometry (Table S1), which agrees with the short spectral profile observed in the MATI spectrum. Figure 2(b) presents the spectral simulation for the $^1\Sigma^+ \leftarrow {}^2\Sigma^+$ transition, where the 0-0 transition is aligned with the experimental origin band, but the computed vibrational frequencies are not scaled for direct comparison with the experiment. As shown in Fig. 2 and Table I, the spectral simulation reproduces nicely the 808 cm^{-1} progression and 785 cm^{-1} hot band, which are attributed to the La^+–N stretch (ν_2^+, σ^+) in the $^1\Sigma^+$ ion and the La–N stretch (ν_2, σ^+) in the $^2\Sigma^+$ ground state. On the other hand, the weak 526 cm^{-1} progression, the 1334 cm^{-1} combination band, and the 458 cm^{-1} hot band are not simulated even though the calculated frequencies for the ν_3^+/ν_3 modes (561/481 cm^{-1}) are in fair agreement with the measured values of 526/458 cm^{-1} for the bending fundamental in the ion and neutral states. The failure to simulate the transitions associated with the odd quantum number change of the bending mode arises from the fact that the bending mode is not totally symmetric and thus forbidden in single photoionization. The previous observation of the bending fundamental in the dispersed fluorescence spectrum was explained in terms of the Renner-Teller effect in the doubly degenerated $C^2\Pi$ state. However, the transition responsible for the MATI spectrum involves only non-degenerated states ($^1\Sigma^+ \leftarrow {}^2\Sigma^+$). Thus, the Renner-Teller effect could not be responsible for the MATI observation. The bending activity may be due to the Herzberg-Teller (HT) effect and/or the anharmonic behavior of the mode. A similar observation has also been observed in the MATI spectrum of a tetrahedron-

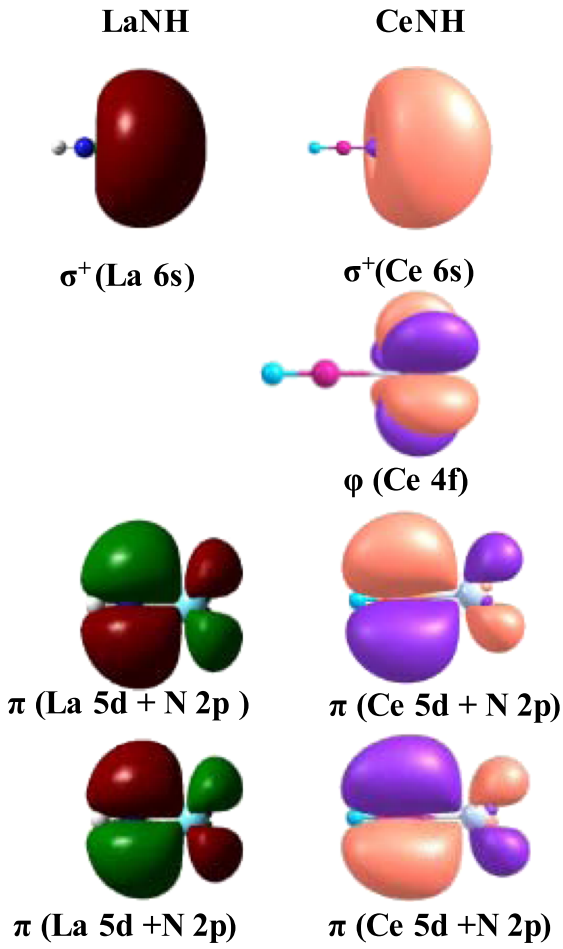

FIG. 3. Valence molecular orbitals of LaNH ($\pi^4(\sigma^+)^1$) (left) and CeNH ($\pi^4\phi^1(\sigma^+)^1$) (right).

TABLE I. Energies (cm^{-1}) of the origin bands and vibrational frequencies (cm^{-1}) of LnNH (Ln = La and Ce) from MATI spectra and theoretical calculations.

Molecule	MATI[a]	Theory[b]	Mode description
LaNH ($C_{\infty v}$, $^1\Sigma^+ \leftarrow {}^2\Sigma^+$)			
Origin band	40 883	41 321	
$\nu_2^+/\nu_2(\sigma^+)$	808/763	840/780 (833/776)	La–N stretch
$\nu_3^+/\nu_3(\pi)$	526/458	565/502 (540/460)	La–N–H bend
CeNH ($C_{\infty v}$, $E_{5/2} \leftarrow \Delta$ (S ≈ 1), Φ)			
Origin band	41 496/41 421	40 590/40 512	
$\nu_2^+/\nu_2(\sigma^+)$	818/	852/794	Ce–N stretch
$\nu_3^+/\nu_3(\pi)$	530/	563/492	Ce–N–H bend

[a]The uncertainty for the adiabatic ionization energies (AIEs) is ~5 cm^{-1}.
[b]For LaNH, the energy of the origin band and vibrational frequencies are from the DFT/B3LYP calculations, and the values in parentheses are anharmonic frequencies. For CeNH, the energies of the origin bands are from the SO-MCQDPT calculations with vibrational zero-point corrections from the DFT/B3LYP calculations.

like trimethylenemethanelanthanum [La(C(CH$_2$)$_3$)].[57] The HT effect may induce an activity of a non-totally symmetry mode in an allowed electronic transition and lead to intensity stealing of the asymmetric vibration from a nearby electronic state. In the current case, the vibronic species with one quantum excitation of the π bending mode in the $^1\Sigma^+$ ion is $^1\Pi^{ev}$, where the superscript "ev" stands for the vibronic state. Then, the direct product of $\Gamma(\Sigma^+) \otimes \Gamma(\Pi)$ has the same irreducible representation as the electric dipole moment along the (x, y) directions, and thus the $^1\Pi^{ev} \leftarrow {}^2\Sigma^+$ transition is symmetry allowed. The $^1\Pi^{ev}$ vibronic state can be coupled to a nearby electronic state of the same symmetry, resulting in the intensity stealing of the $^1\Pi^{ev} \leftarrow {}^2\Sigma^+$ vibronic transition from the $^1\Pi \leftarrow {}^2\Sigma^+$ allowed electronic transition. The $^1\Pi$ ion state could be formed by the removal of a π electron from the ground electron configuration ($\pi^4(\sigma^+)^1$) of the neutral molecule. The energy difference between the $^1\Pi$ and $^1\Sigma^+$ ion states is roughly estimated to be 2.6 eV by the energy difference of the π^4 and $(\sigma^+)^1$ orbital. Because the $^1\Pi$ and $^1\Pi^{ev}$ states are quite apart in energy, their coupling is expected to be relatively weak. Similar discussion applies to the observation of the thermally excited bending fundamental of the $^2\Sigma^+$ ground state of the neutral molecule, where the $^1\Sigma^+ \leftarrow {}^2\Pi^{ev}$ vibronic transition steals intensity from the $^1\Sigma^+ \leftarrow {}^2\Pi$ allowed electronic transition. The previous fluorescence study reported that the C$^2\Pi$ state is ~23 000 cm^{-1} above the $^2\Sigma^+$ ground state of the molecule.[29] To investigate the anharmonic behavior of the molecular vibrations, we calculated the anharmonic vibrational frequencies, which are listed in Table I in comparison with the harmonic and experimental values. While the harmonic and anharmonic stretching fundamental are very similar, the anharmonic bending frequency is significantly smaller than the harmonic value and has better agreement with the measured value.

Other transitions of LaNH and ionization of NLaH are excluded from the observed MATI spectrum. In addition to the $^1\Sigma^+ \leftarrow {}^2\Sigma^+$ transition of LaNH, we have also considered the $^3\Sigma^+ \leftarrow {}^2\Sigma^+$ and $^3\Sigma^+ \leftarrow {}^4A'$ transitions. However, the $^3\Sigma^+ \leftarrow {}^2\Sigma^+$ transition is predicted to have a much higher IE (62 586 cm^{-1}) than the observed value (40 883 cm^{-1}), whereas the $^4A''$ state is ~21 000 cm^{-1} higher in energy than the $^2\Sigma^+$ ground state (Table S1). NLaH is much less stable than LaNH, and the IE of the doublet ground state is much higher than the experimental value (Table S1). Therefore, NLaH may not be formed in the molecular beam or may be quenched by the supersonic expansion.

C. Two band systems of CeNH

The MATI spectrum of CeNH [Fig. 4(a)] shows two strong bands at 41 421 (5) and 41 496 (5) cm^{-1}. Associated with each of the strong bands are a short 818 cm^{-1} progression with up to two quanta and a weak band at 530 cm^{-1} on the higher energy side. Additionally, the spectrum displays a weak band at 646 cm^{-1} (marked with "*") above the 41 496 cm^{-1} strong band. The 818 and 530 cm^{-1} transitions could easily be assigned to the Ce$^+$–N stretching and N–Ce$^+$–H bending vibrations in the ion. The stronger band at 41 496 cm^{-1} is the origin band of an electronic transition, while the weaker band at 41 421 cm^{-1} could be the origin band of another

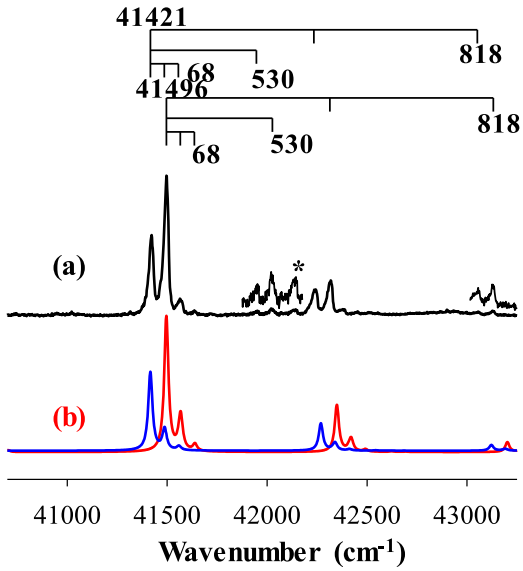

FIG. 4. MATI spectrum (a) and simulation of $^2\Phi \leftarrow {}^3\Phi$ at 350 K (b) of CeNH. The energies and intensities of the calculated origin bands are aligned with or normalized to those of the experimental origin bands.

electronic transition or a hot band originating from a thermally excited vibrational level of the neutral molecule to the zero- or first vibrational level of the ion. However, the assignment of the 41 421 cm^{-1} band to a transition associated with a thermally excited vibrational mode of the neutral molecule would imply that the neutral mode has a vibrational frequency of 75 cm^{-1} or the neutral mode is 75 cm^{-1} larger than the corresponding ion mode (i.e., sequence transition). Either of the two possibilities can be excluded because no neutral vibrational mode of the molecule is expected to have such a low frequency or have a higher frequency than the corresponding ion mode as demonstrated by the MATI spectrum of LaNH. Thus, the MATI spectrum of CeNH must consist of two band systems, which could arise from the ionization of two isomers or two electronic states or SO levels of a single isomer. To attempt to identify the two band systems, we first carried out DFT calculations on CeNH and NCeH by following the same approach as the one used for the La species. Our DFT calculations show that CeNH ($^3\Phi$) is more stable than the NCeH ($^1A'$) by almost 1 eV, and a singlet excited state of CeNH ($^1\Sigma^+$) is less stable than the triplet ground state by more than 1 eV (Table S1). Thus, the two band systems observed in the MATI spectrum are unlikely associated with two isomers of the Ce species or the excited $^1\Sigma^+$ state of CeNH. The explanation of the two band systems thus requires more sophisticated calculations that include multiconfiguration or SO coupling.

To investigate further transitions responsible for the observed two band systems, we have carried out two separate calculations on CeNH and CeNH$^+$: multiconfiguration without and with SO coupling. Although the ground state of Ce has the electron configuration $4f^1 5d^1 6s^2$, the Ce-based electron configuration of CeNH is $4f^1 6s^1$. The remaining two electrons that are associated with the isolated Ce atom are in a doubly degenerated orbital that is a bonding combination between Ce $5d_\pi$ and N $p_{x,y}$ with the z-axis being collinear with the molecular axis (Fig. 3). Because there are seven 4f orbitals in a Ce atom,

the coupling of the 4f and 6s orbitals should form seven triplets if the two electrons are in the same spin and seven singlets if their spins are opposite. The removal of the Ce $6s^1$ electron yields seven doublet ion states. State-averaged MCSCF calculations predict the seven triplets to be within 0.19 eV, the seven singlets 0.26 eV, and the seven doublets 0.14 eV. In each spin, the seven states consist of one non-degenerate and three doubly degenerate states. The state degeneracy is governed by the reduced representations of the 4f orbitals in the $C_{\infty v}$ point group, which are σ^+ for $4f_0$, π for $4f_{\pm1}$, δ for $4f_{\pm2}$, and ϕ for $4f_{\pm3}$. The slight energy differences among the seven states of each spin are associated with the different orientations and lobes of the seven 4f orbitals. Dynamic electron correlation is added to MCSCF by MCQDPT calculations. The energies of the first few lowest states of the neutral molecule and cation are listed in Table II. The table shows that including the dynamic electron correlation reduces the energy differences among the low-energy states of the neural molecule and cation. However, the energy difference between the two lowest states of the neutral molecule (or the cation) is still three times as large as the observed separation of the two band systems (75 cm^{-1}). Thus, the two band systems are neither due to the transitions from the $^3\Phi$ and $^1\Phi$ states of the molecule to the lowest-energy $^2\Phi$ state of the cation, which would produce a 216 cm^{-1} separation of the two band systems, nor due to the transitions from the $^3\Phi$ state of the neutral molecule to the $^2\Phi$ and $^2\Delta$ states of the ion, which would produce a 494 cm^{-1} separation between the two band systems, both at the MCQDPT level. Furthermore, the thermally excited singlet state of the neutral molecule would have a considerably smaller population to produce the observed intensity of the lower-energy band system [I(41 421 cm^{-1})/I(41 496 cm^{-1}) ≈ 60 %] in the molecular beam. If the transitions were from the $^3\Phi$ state of the neutral molecule to the two doublet states of the ion, the two band systems would show similar intensities because the excitation of a neutral ground state to two ion states with similar electron configurations (i.e., $4f^1$) should have comparable ionization cross sections.

The most likely explanation for the observed 75 cm^{-1} splitting of the two band systems is the SO coupling between the Ce $4f^1$ and $6s^1$ orbitals of the neutral molecule. Table II shows relative energies of several lowest-energy SO coupled levels. The energy difference between the Δ (S ≈ 1) and Φ SO terms are predicted to be 78 cm^{-1} at the SO-MCQDPT level, which is in excellent agreement with the experiment. A similar agreement between the SO-MCQDPT calculation and the MATI measurement was also obtained for $Ce(C_2H_2)$.[58] Moreover, the inclusion of all but the deep core correlation energy gives 40 590 cm^{-1} for the higher origin band at the SO-MCQDPT level, agreeing reasonably with the origin band observed at 41 496 cm^{-1}. In Table II, the SO coupled level symmetries are the overall symmetry products of the electron spin and spatial symmetries. To have a nonzero SO coupling matrix element $\int \psi_1(o)\psi_1(s)|H_{so}|\psi_2(o)\psi_2(s)d\tau$, the direct product of $\Gamma_1(o)\ \Gamma_1(s) \otimes \Gamma(H_{so}) \otimes \Gamma_2(o)\ \Gamma_2(s)$ will contain the totally symmetric representation, where $\Gamma_{1,2}(o)\ \Gamma_{1,2}(s)$ are representations of the spatial and spin symmetries of states 1 and 2, and $\Gamma(H_{so})$ is the representation of the SO Hamiltonian operator. Because the $\Gamma(H_{so})$ belongs to the totally symmetric representation, the direct product of $\Gamma_1(o)\ \Gamma_1(s) \otimes \Gamma_2(o)\ \Gamma_2(s)$ must contain the totally symmetric representation, or $\Gamma_1(o)\ \Gamma_1(s)$ must contain or be the same representation as $\Gamma_2(o)\ \Gamma_2(s)$ for a nonzero SO matrix element. Under $C_{\infty v}$, the representation of a singlet spin state is Σ^+ and those of a triplet spin state are $\Sigma^- + \Pi$.[59] As an example, we consider the symmetry label for the 78 cm^{-1} SO level, which consists of $^3\Phi$ (91%), $^3\Delta$ (6%), and $^1\Delta$ (3%) spatial terms. The symmetry direct products of the $^3\Phi$, $^3\Delta$, and $^1\Delta$ spatial terms and the respective triplet and singlet spin terms are $\Phi \otimes (\Sigma^- + \Pi) = \Phi + \Delta + \Gamma$, $\Delta \otimes (\Sigma^- + \Pi) = \Delta + \Pi + \Phi$, and $\Delta \otimes \Sigma^+ = \Delta$, respectively. The SO level symmetry thus must be Δ to yield a nonzero SO matrix element.

With the identification of the SO levels as the contributors for the observed 75 cm^{-1} splitting, we now turn our attention to the spectral simulations. We use the spatial $^3\Phi$ state to represent the initial neutral state and the $^2\Phi$ state for the final ion state to simulate the observed MATI spectrum. We do so because the SO coupled levels are made of these states. A SO electronic temperature of ~200 K was estimated from the relative intensities of the two origin bands. This temperature is

TABLE II. Lowest electronic terms before spin–orbit (SO) coupling, the lowest SO coupled levels, and adiabatic ionization energies (AIEs) of CeNH from relativistic *ab initio* calculations (all expressed in cm^{-1}). The AIEs included zero-point energy correction that calculated by the DFT/B3LYP calculations.

	Without SO coupling			With SO coupling		
Term	MCSCF	MCQDPT	SO-term	SO-MCSCF	SO-MCQDPT	Term contribution
CeNH						
$^3\Phi$	0	0	Δ (S ≈ 1)	0	0	91% $^3\Phi$, 6% $^3\Delta$, 3% $^1\Delta$
$^1\Phi$	356	216	Φ	132	78	40% $^1\Phi$, 50% $^3\Phi$, 9%$^3\Delta$
$^3\Delta$	673	606	Π (S ≈ 1)	808	737	84% $^3\Delta$, 13% $^3\Pi$, 3% $^1\Pi$
$^1\Delta$	1150	949	Δ	940	827	35% $^1\Delta$, 45% $^3\Delta$, 19% $^3\Pi$
$CeNH^+$						
$^2\Phi$	0	0	$^2E_{5/2}$	0	0	90% $^2\Phi$, 10% $^2\Delta$
$^2\Delta$	538	494	$^2E_{3/2}$	642	600	82% $^2\Delta$, 9% $^2\Pi$, 9% $^2\Sigma^+$
$^2\Pi$	1 245	1 190	$^2E_{1/2}$	1 148	1 065	73% $^2\Delta$, 27% $^2\Sigma^+$
AIE	38 044	40 607		38 018	40 590	

different from that (350 K) used for simulating the vibrational hot bands. Clearly, the simulation [Fig. 4(b)] reproduces the 818 cm^{-1} progression that is attributed to the Ce^+–N stretching excitations in the ion and the 68 cm^{-1} sequence bands that are associated with the bending mode in the neutral molecule and the ion. The 530 cm^{-1} is not simulated but assigned to the excitation of the Ce^+–N–H bending excitation, similar to the case of LaNH. The very weak band at 646 cm^{-1} above the 41 496 cm^{-1} origin band could not be accounted for by the simulations, and no corresponding band is observed in the MATI spectrum of LaNH. This band may be due to the transition from the lowest SO level ($\Delta, S \approx 1$) of the neutral molecule to the second lowest SO level ($^2E_{3/2}$) of the ion. This assignment gives a computed band at 600 cm^{-1} above the origin band, which is in reasonably good agreement with the observed band at 646 cm^{-1}, but it does not explain the weak intensity of the observed band. A second possibility is to assign this band to the transition from the second SO level (Φ) of the neutral molecule to the second SO level ($^2E_{3/2}$) of the ion, which yields a theoretical transition at 522 cm^{-1} above the origin band. This assignment explains better the observed weak intensity, though the calculated transition energy is considerably lower (by 124 cm^{-1}) than the experiment. In either case, the assignment of this band is uncertain.

D. Formation of LnNH (Ln = La and Ce)

LnNH (Ln = La and Ce) is formed by Ln-mediated dehydrogenation of ammonia. Because the pathways for the formation of both LaNH and CeNH are very similar (Fig. 5 and Table S2), we will focus on one of the species, LaNH. The first step is La addition to NH_3 to form an association complex, $LaNH_3$ (IM1). The Ln association has a very small perturbation to the structure of ammonia as shown by the nearly

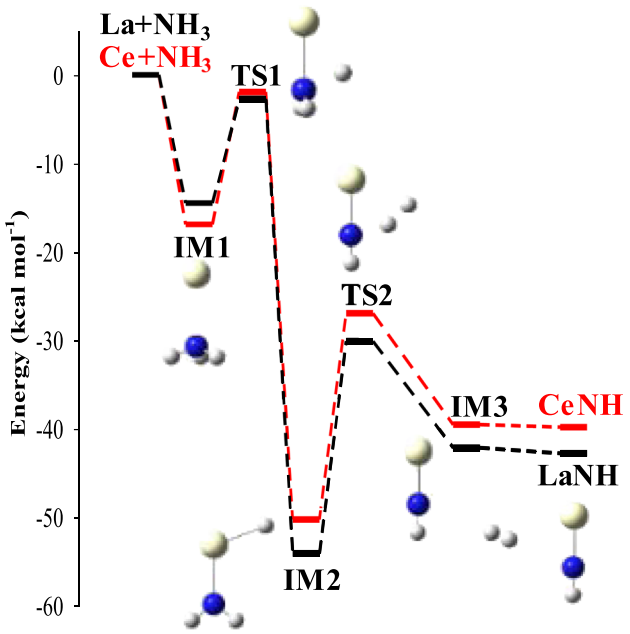

FIG. 5. Reaction pathways and energy profiles for the formation of LaNH ($^2\Sigma^+$) (black trace) and CeNH ($^3\Phi$) (red trace) from La/Ce + NH_3 reactions calculated at the DFT/B3LYP level, where IMn stands for intermediates and TSn stands for transition states.

identical N–H bond lengths in the coordinated and free NH_3 (1.024 Å in $LaNH_3$ and 1.015 Å in NH_3). It should be noted that the La–NH_3 bonding is different from La–C_2H_4, where the C–C π bond is cleaved upon La addition, and sp^2 carbons are transformed to sp^3 carbons.[60] The bonding difference arises from a largely electrostatic interaction (i.e., a dipole-induced diploe interaction) in La–NH_3 and an orbital interaction in La–C_2H_4. The second step involves the activation of two N–H bonds. The first N–H activation is through La insertion into a N–H bond to form an inserted complex, $HLaNH_2$ (IM2), which is more stable than the adduct $LaNH_3$. The enhanced stability of the inserted species is due to the formation of two new bonds (La–H and La–N) that overcompensates the loss of the N–H bond. The transition state (TS1) connecting the adduct and inserted species is characterized by an imaginary N–H stretching vibration (1412i cm^{-1}) with H being migrated to La. The second N–H activation proceeds by the formation of a dihydrogen complex, (H_2)LaNH (IM3), through the transition state TS2 where H in the activated N–H bond migrates toward the La-bound H. (H_2)LaNH is a dihydrogen rather than dihydride complex because the H–H distance (0.745 Å) in the complex is almost the same as that in a free H_2 molecule (0.744 Å). (H_2)LaNH is less stable than $HLaNH_2$ because the cleavage of the La–H and N–H bonds requires more energy than that released from the formation of the H–H bond. The last step is the decomposition of H_2LaNH into LaNH and H_2. As H_2 is essentially nonbonding with LaNH in the complex, the decomposition reaction does not encounter any barrier. The overall reaction La + NH_3 → LaNH + H_2 is barrierless and exothermic by 42.7 kcal mol^{-1}. The energy profile for the Ce + NH_3 → CeNH + H_2 reaction is very similar to that of the La reaction (Table S2), which is also barrierless and exothermic (by 39.8 kcal mol^{-1}). Previously, the Ce + NH_3 reaction in solid Ar matrices was reported to yield NCeH.[38,39] It is noted that predicted reaction pathways for the formation of the two Ce isomers are the same up to $HCeNH_2$ (IM2) and then diverge afterwards. For the formation of NCeH, the second N–H activation produces a dihydride complex, rather than a dihydrogen species as in the case of CeNH.

IV. CONCLUSION

LnNH (Ln = La and Ce) formed by the Ln + NH_3 reactions are characterized by MATI spectroscopy and quantum chemical calculations. The spectrum of LaNH displays a single band system consisting of vibronic transitions associated with the La^+/La–N stretching and La^+/La–N–H bending excitations in the $^1\Sigma^+$ cation and the $^2\Sigma^+$ neutral molecule, respectively. The valence electron configuration of $^2\Sigma^+$ is La $6s^1$, and the ionization of the La-based 6s electron yields the $^1\Sigma^+$ ion. The spectrum of CeNH exhibits two band systems, each showing the stretching and bending activities like that of LaNH. The low-energy valence electron configurations of the neutral molecule and ion species are Ce $4f^16s^1$ and Ce $4f^1$. The two band systems arise from the transitions of the two lowest SO levels of the neutral molecule to the lowest SO level of the ion. The SO coupling occurs between the Ce $4f^1$ and $6s^1$ electrons. The lower SO level consists of nearly all triplet terms, while the higher level is a heavy mixture of the triplet and singlet

terms. The formation of both LnNH molecules proceeds with exothermically concerted H_2 elimination without any energy barriers. Additional studies on Ln reactions with simple amines would be interesting as they could explore the competition of the N–H and C–H bond activation and degrees of SO coupling in nonlinear Ln radicals.

SUPPLEMENTARY MATERIAL

See supplementary material for the geometries of LaNH and CeNH in various spin states and electronic energies including vibrational zero-point corrections of the stationary points along the reaction coordinates for the formation of the two species.

ACKNOWLEDGMENTS

We are grateful for the financial support from the National Science Foundation Division of Chemistry (Chemical Structure, Dynamics, and Mechanisms, Grant No. 1800316) and to Dr. Michael Schmidt for his help in relativistic calculations using the GAMESS quantum chemistry package.

[1] J. Zhao, A. S. Goldman, and J. F. Hartwig, Science **307**, 1080 (2005).
[2] J. L. Klinkenberg and J. F. Hartwig, Angew. Chem., Int. Ed. **50**, 86 (2011).
[3] F. Collet, R. H. Dodd, and P. Dauban, Chem. Commun. **2009**, 5061.
[4] D. Hazelard, P.-A. Nocquet, and P. Compain, Org. Chem. Front. **4**, 2500 (2017).
[5] R. Lan, J. T. S. Irvine, and S. Tao, Int. J. Hydrogen Energy **37**, 1482 (2012).
[6] R. Kretschmer, M. Schlangen, and H. Schwarz, Dalton Trans. **42**, 4153 (2013).
[7] R. Kretschmer, M. Schlangen, M. Kaupp, and H. Schwarz, Organometallics **31**, 3816 (2012).
[8] R. Kretschmer, X. H. Zhang, M. Schlangen, and H. Schwarz, Chem. Eur. J. **17**, 3886 (2011).
[9] R. Liyanage and P. B. Armentrout, Int. J. Mass Spectrom. **241**, 243 (2005).
[10] V. Blagojevic, V. V. Lavrov, G. K. Koyanagi, and D. K. Bohme, Int. J. Mass Spectrom. **413**, 81 (2017).
[11] G. K. Koyanagi, P. Cheng, and D. K. Bohme, J. Phys. Chem. **114**, 241 (2010).
[12] A. Quemet, P. Vitorge, A. Cimas, S. S. Li, J. Y. Salpin, C. Marsden, J. Tortajada, L. Gagliardi, R. Spezia, M. P. Gaigeot, and R. Brennetot, Int. J. Mass Spectrom. **334**, 27 (2013).
[13] G. K. Koyanagi, V. Kapishon, D. K. Bohme, X. H. Zhang, and H. Schwarz, Eur. J. Inorg. Chem. **2010**, 1516.
[14] D. E. Clemmer and P. B. Armentrout, J. Phys. Chem. **95**, 3084 (1991).
[15] S. W. Buckner, J. R. Gord, and B. S. Freiser, J. Am. Chem. Soc. **110**, 6606 (1988).
[16] D. E. Clemmer, L. S. Sunderlin, and P. B. Armentrout, J. Phys. Chem. **94**, 3008 (1990).
[17] R. Kretschmer, M. Schlangen, and H. Schwarz, Chem. Eur. J. **18**, 40 (2012).
[18] D. S. Yang and J. Miyawaki, Chem. Phys. Lett. **313**, 514 (1999).
[19] G. K. Rothschopf, J. S. Perkins, S. Li, and D.-S. Yang, J. Phys. Chem. A **104**, 8178 (2000).
[20] S. G. Li, G. K. Rothschopf, D. Pillai, B. R. Sohnlein, B. M. Wilson, and D. S. Yang, J. Chem. Phys. **115**, 7968 (2001).
[21] J. Miyawaki, D. S. Yang, and K. Sugawara, Chem. Phys. Lett. **372**, 627 (2003).
[22] S. G. Li, B. R. Sohnlein, D. S. Yang, J. Miyawaki, and K. I. Sugawara, J. Chem. Phys. **122**, 214316 (2005).
[23] J. Miyawaki, S. Djafari, K. Sugawara, and H. Takeo, J. Chem. Phys. **118**, 8 (2003).
[24] J. Miyawaki and K. Sugawara, J. Chem. Phys. **119**, 6539 (2003).
[25] B. Simard, D. M. Rayner, E. Benichou, N. Mireles, F. J. Tenorio, and A. Martinez, J. Phys. Chem. A **107**, 9099 (2003).
[26] B. Simard, Z. Jakubek, H. Niki, and W. J. Balfour, J. Chem. Phys. **111**, 1483 (1999).
[27] Z. J. Jakubek, B. Simard, H. Niki, and W. J. Balfour, J. Chem. Phys. **113**, 3591 (2000).
[28] T. C. Steimle, J. Xin, A. J. Marr, and S. Beaton, J. Chem. Phys. **106**, 9084 (1997).
[29] S. Bhattacharyya, S. Mukund, and S. G. Nakhate, Chem. Phys. Lett. **692**, 1 (2018).
[30] T. C. Steimle, R. R. Bousquet, A. J. Merer, and S. J. Rixon, J. Chem. Phys. **118**, 1266 (2003).
[31] D. V. Lanzisera and L. Andrews, J. Phys. Chem. A **101**, 5082 (1997).
[32] M. Zhou, M. Chen, L. Zhang, and H. Lu, J. Phys. Chem. A **106**, 9017 (2002).
[33] M. Chen, H. Lu, J. Dong, L. Miao, and M. Zhou, J. Phys. Chem. A **106**, 11456 (2002).
[34] X. Wang and L. Andrews, Organometallics **27**, 4885 (2008).
[35] X. Liu, X. Wang, B. Xu, and L. Andrews, Chem. Phys. Lett. **523**, 6 (2012).
[36] X. Wang, L. Andrews, and C. J. Marsden, Chem. - Eur. J. **13**, 5601 (2007).
[37] X. Wang, L. Andrews, and C. J. Mardsden, Chem. - Eur. J. **14**, 9192 (2008).
[38] Z. Pu, W. Yu, S. K. Roy, C. Li, B. Ao, T. Liu, M. Shuai, and X. Wang, Phys. Chem. Chem. Phys. **19**, 8216 (2017).
[39] Z. Pu, F. Li, J. Qin, B. Ao, P. Shi, and M. Shuai, J. Phys. Chem. A **122**, 3541 (2018).
[40] S. Cotton, *Lanthanide and Actinide Chemistry* (John Wiley & Sons, West Sussex, England, 2006).
[41] B. R. Sohnlein, S. G. Li, J. F. Fuller, and D.-S. Yang, J. Chem. Phys. **123**, 014318 (2005).
[42] M. J. Frish, G. W. Trucks, H. B. Schlegel, G. E. Scuseria, M. A. Robb, J. R. Cheeseman, G. Scalmani, V. Barone, B. Mennucci, G. A. Petersson, H. Nakatsuji, M. Caricato, X. Li, H. P. Hratchian, A. F. Izmaylov, J. Bloino, and G. Zheng, GAUSSIAN 09, Revision A.01, Gaussian, Inc., Wallingford, CT, 2009.
[43] S. Li, "Threshold photoionization and ZEKE photoelectron spectroscopy of metal complexes," Ph.D. thesis, University of Kentucky, 2004.
[44] J. Seino and H. Nakai, J. Chem. Phys. **136**, 244102 (2012).
[45] M. Barysz and A. J. Sadlej, J. Chem. Phys. **116**, 2696 (2002).
[46] D. Kedziera and M. Barysz, J. Chem. Phys. **121**, 6719 (2004).
[47] T. Noro, M. Sekiya, and T. Koga, Theoret. Chem. Acc. **131**, 1124 (2012).
[48] M. Sekiya, T. Noro, and T. Koga, Theoret. Chem. Acc. **131**, 1247 (2012).
[49] P. Piecuch, J. R. Gour, and M. Wloch, Int. J. Quantum Chem. **109**, 3268 (2009).
[50] K. R. Glaesemann and M. W. Schmidt, J. Phys. Chem. A **114**, 8772 (2010).
[51] M. W. Schmidt and M. S. Gordon, Ann. Rev. Phys. Chem **49**, 233 (1998).
[52] H. Nakano, J. Chem. Phys. **99**, 7983 (1993).
[53] D. G. Fedorov and J. P. Finley, Phys. Rev. A **64**, 042502 (2002).
[54] D. G. Fedorov, S. Koseki, M. W. Schmidt, and M. S. Gordon, Int. Rev. Phys. Chem. **22**, 551 (2003).
[55] D. G. Fedorov and M. S. Gordon, J. Chem. Phys. **112**, 5611 (2000).
[56] M. W. Schmidt, K. K. Baldridge, J. A. Boatz, S. T. Elbert, M. S. Gordon, J. J. Jensen, S. Koseki, N. Matsunaga, K. A. Nguyen, S. Su, T. L. Windus, M. Dupuis, and J. A. Montgomery, J. Comput. Chem. **14**, 1347 (1993).
[57] D. Hewage, W. Cao, S. Kumari, R. Silva, T. H. Li, and D.-S. Yang, J. Chem. Phys. **146**, 184304 (2017).
[58] Y. Zhang, M. W. Schmidt, S. Kumari, M. S. Gordon, and D.-S. Yang, J. Phys. Chem. A **120**, 6963 (2016).
[59] G. Herzberg, *Molecular Spectra and Molecular Structure, Volume III: Electronic Spectra and Electronic Structure of Polyatomic Molecules* (Krieger, Malabar, FL, 1991).
[60] S. Kumari, W. Cao, Y. Zhang, M. Roudjane, and D.-S. Yang, J. Phys. Chem. A **120**, 4482 (2016).